PHYS414/514 Final Project: Stars, from Newton to Einstein

Cafer Halim Baytok
Department of Physics, Koç University,
Rumelifeneri Yolu, 34450 Sarıyer, Istanbul, Turkey
(Dated: January 2026)

We study the structure of compact stars within Newtonian gravity and general relativity. In the Newtonian framework, we derive the Lane–Emden equation for polytropic equations of state, analyze its regular solutions, and obtain mass–radius scaling relations. We then compare the polytropic predictions with observational white dwarf data and extend the modeling by using the full cold degenerate-electron equation of state, solving the Newtonian structure equations by direct numerical integration and fitting the equation-of-state parameter D to the data. Finally, we model neutron stars in general relativity via the Tolman–Oppenheimer–Volkoff equations, compute the mass–radius relation, identify the maximum mass and stability boundary, and quantify gravitational binding effects through the proper mass.

NEWTON

Lane–Emden Derivation

We start from the Newtonian stellar structure equations for a spherically symmetric configuration:

$$\frac{dm}{dr} = 4\pi r^2 \rho(r), \qquad \frac{dp}{dr} = -\frac{Gm(r)\rho(r)}{r^2}. \tag{1}$$

We also assume a polytropic equation of state (EOS)

$$p = K\rho^{\gamma} = K\rho^{1+\frac{1}{n}}, \tag{2}$$

where K is a constant and n is the polytropic index.

Step 1: Put the equations into a single second-order form

Starting from hydrostatic equilibrium, divide by ρ and multiply by r^2:

$$\frac{r^2}{\rho}\frac{dp}{dr} = -Gm(r). \tag{3}$$

Now differentiate both sides with respect to r:

$$\frac{d}{dr}\left(\frac{r^2}{\rho}\frac{dp}{dr}\right) = -G\frac{dm}{dr}. \tag{4}$$

Using mass conservation $\frac{dm}{dr} = 4\pi r^2\rho$, we obtain

$$\frac{d}{dr}\left(\frac{r^2}{\rho}\frac{dp}{dr}\right) = -4\pi G r^2 \rho. \tag{5}$$

Finally, divide by r^2 to arrive at a compact second-order equation:

$$\frac{1}{r^2}\frac{d}{dr}\left(\frac{r^2}{\rho}\frac{dp}{dr}\right) = -4\pi G\rho. \tag{6}$$

Step 2: Use the polytropic EOS to rewrite derivatives

From

$$p(\rho) = K\rho^{1+\frac{1}{n}}, \tag{7}$$

we compute

$$\frac{dp}{d\rho} = K\left(1+\frac{1}{n}\right)\rho^{\frac{1}{n}} = (n+1)K\,\rho^{\frac{1}{n}}. \tag{8}$$

By the chain rule,

$$\frac{dp}{dr} = \frac{dp}{d\rho}\frac{d\rho}{dr} = (n+1)K\,\rho^{\frac{1}{n}}\frac{d\rho}{dr}. \tag{9}$$

Therefore,

$$\frac{1}{\rho}\frac{dp}{dr} = (n+1)K\,\rho^{\frac{1}{n}-1}\frac{d\rho}{dr}. \tag{10}$$

Step 3: Introduce dimensionless variables

Let $\rho_c \equiv \rho(0)$ be the central density, and define a dimensionless function $\theta(\xi)$ via

$$\rho(r) = \rho_c\,\theta(\xi)^n. \tag{11}$$

This implies $\theta(0) = 1$.

Next define a dimensionless radius ξ by

$$r = a\xi, \qquad a^2 \equiv \frac{(n+1)K}{4\pi G}\,\rho_c^{\frac{1}{n}-1}. \tag{12}$$

Step 4: Substitute and reduce to Lane–Emden

Differentiate (11):

$$\frac{d\rho}{dr} = \rho_c\, n\,\theta^{n-1}\frac{d\theta}{dr}. \tag{13}$$

Insert this into (10). Note that

$$\rho^{\frac{1}{n}-1} = (\rho_c\theta^n)^{\frac{1}{n}-1} = \rho_c^{\frac{1}{n}-1}\theta^{1-n}. \tag{14}$$

Hence

$$\frac{1}{\rho}\frac{dp}{dr} = (n+1)K\,n\,\rho_c^{\frac{1}{n}}\frac{d\theta}{dr}. \tag{15}$$

Plugging into (6) yields

$$(n+1)K\,n\,\rho_c^{\frac{1}{n}}\frac{1}{r^2}\frac{d}{dr}\left(r^2\frac{d\theta}{dr}\right) = -4\pi G\rho_c\theta^n. \tag{16}$$

Divide both sides by $(n+1)K\,n\,\rho_c^{\frac{1}{n}}$:

$$\frac{1}{r^2}\frac{d}{dr}\left(r^2\frac{d\theta}{dr}\right) = -\frac{4\pi G\rho_c}{(n+1)K\,n\,\rho_c^{\frac{1}{n}}}\,\theta^n. \tag{17}$$

Now use $r = a\xi$ and $d/dr = (1/a)\,d/d\xi$. Then

$$\frac{1}{r^2}\frac{d}{dr}\left(r^2\frac{d\theta}{dr}\right) = \frac{1}{a^2\xi^2}\frac{d}{d\xi}\left(\xi^2\frac{d\theta}{d\xi}\right). \tag{18}$$

With the choice of a in (12), the prefactor becomes exactly -1, and we obtain the Lane–Emden equation:

$$\frac{1}{\xi^2}\frac{d}{d\xi}\left(\xi^2\frac{d\theta}{d\xi}\right) + \theta^n = 0. \tag{19}$$

The central boundary condition is

$$\theta(0) = 1. \tag{20}$$

Series Expansion at the Center and Regularity

After deriving the Lane–Emden equation in dimensionless form,

$$\frac{1}{\xi^2}\frac{d}{d\xi}\left(\xi^2\frac{d\theta}{d\xi}\right) + \theta^n = 0, \tag{21}$$

the behavior of the solution near the center $\xi = 0$ must be analyzed. Although the equation appears singular due to the explicit $1/\xi^2$ factor, this singularity is not physical. A physically acceptable solution must remain finite and smooth at the center.

To study the regular behavior, we expand the solution around $\xi = 0$ as a power series using *Mathematica*. Regularity excludes odd powers of ξ, since such terms would produce a nonvanishing first derivative at the origin and lead to divergent contributions through the $(2/\xi)\theta'(\xi)$ term. Therefore, the expansion must contain only even powers of ξ:

$$\theta(\xi) = 1 + a\,\xi^2 + b\,\xi^4 + \mathcal{O}(\xi^6), \tag{22}$$

where the normalization $\theta(0) = 1$ has been imposed.

Substituting this expansion into the Lane–Emden equation and matching powers of ξ order by order uniquely determines the coefficients. At leading order, one finds

$$a = -\frac{1}{6}, \tag{23}$$

while the next-order coefficient depends explicitly on the polytropic index n,

$$b = \frac{n}{120}. \tag{24}$$

Hence, the regular solution near the center behaves as

$$\boxed{\theta(\xi) = 1 - \frac{\xi^2}{6} + \frac{n}{120}\,\xi^4 + \mathcal{O}(\xi^6)}. \tag{25}$$

From this expansion it follows immediately that

$$\theta'(0) = 0, \tag{26}$$

which is not imposed as an independent boundary condition, but arises naturally from the requirement of regularity at the center.

Analytic Solution for $n = 1$

For the special case $n = 1$, the Lane–Emden equation admits an exact analytic solution. Solving the equation yields

$$\theta(\xi) = \frac{\sin\xi}{\xi}, \tag{27}$$

which is manifestly regular at the origin. Expanding this solution around $\xi = 0$ gives

$$\frac{\sin\xi}{\xi} = 1 - \frac{\xi^2}{6} + \frac{\xi^4}{120} + \mathcal{O}(\xi^6). \tag{28}$$

This expansion exactly reproduces the general series solution obtained above for $n = 1$, confirming the consistency between the series analysis and the exact analytic solution.

Mass at the Surface and the Mass–Radius Relation

If the Lane–Emden variables are introduced correctly, one has

$$\rho(r) = \rho_c\,\theta(\xi)^n, \qquad r = a\xi, \tag{29}$$

and the stellar surface corresponds to the first zero ξ_n such that

$$\theta(\xi_n) = 0 \iff \rho(R) = 0, \qquad R = a\xi_n. \tag{30}$$

Derivation of the total mass formula

The enclosed mass is

$$m(r) = 4\pi \int_0^r r'^2 \rho(r')\, dr'. \tag{31}$$

Changing variables to ξ using $r = a\xi$ and $dr = a\, d\xi$ gives

$$m(\xi) = 4\pi a^3 \rho_c \int_0^{\xi} \xi'^2 \theta(\xi')^n\, d\xi'. \tag{32}$$

Thus the total mass is

$$M = m(\xi_n) = 4\pi a^3 \rho_c \int_0^{\xi_n} \xi'^2 \theta(\xi')^n\, d\xi'. \tag{33}$$

Now use the Lane–Emden equation

$$\frac{1}{\xi^2}\frac{d}{d\xi}\big(\xi^2\theta'(\xi)\big) + \theta(\xi)^n = 0 \Longrightarrow \theta(\xi)^n = -\frac{1}{\xi^2}\frac{d}{d\xi}\big(\xi^2\theta'(\xi)\big)\,. \tag{34}$$

Multiplying by ξ^2 and integrating from 0 to ξ_n yields

$$\int_0^{\xi_n} \xi^2 \theta(\xi)^n\, d\xi = -\Big[\xi^2\theta'(\xi)\Big]_0^{\xi_n}. \tag{35}$$

Regularity at the center implies $\xi^2\theta'(\xi) \to 0$ as $\xi \to 0$, hence

$$\int_0^{\xi_n} \xi^2 \theta(\xi)^n\, d\xi = -\xi_n^2 \theta'(\xi_n). \tag{36}$$

Therefore,

$$M = 4\pi a^3 \rho_c\big(-\xi_n^2\theta'(\xi_n)\big). \tag{37}$$

Using $R = a\xi_n$ (so that $a^3\xi_n^2 = R^3/\xi_n$), we obtain the required form:

$$\boxed{M = 4\pi\rho_c R^3 \left(-\frac{\theta'(\xi_n)}{\xi_n}\right).} \tag{38}$$

Mass–radius scaling for fixed polytropic EOS

For a polytropic EOS, the Lane–Emden scaling length satisfies

$$a^2 = \frac{(n+1)K}{4\pi G}\, \rho_c^{\frac{1}{n}-1}. \tag{39}$$

Hence the radius scales as

$$R = a\xi_n \propto a \propto K^{1/2}\, \rho_c^{\frac{1}{2}\left(\frac{1}{n}-1\right)} = K^{1/2}\, \rho_c^{\frac{1-n}{2n}}.$$

From the mass formula above (or directly from $M \propto \rho_c a^3$), the mass scales as

$$M \propto \rho_c a^3 \propto \rho_c\, K^{3/2}\, \rho_c^{\frac{3(1-n)}{2n}} = K^{3/2}\, \rho_c^{\frac{3-n}{2n}}.$$

Eliminating ρ_c between these two relations gives

$$\boxed{M \propto R^{\frac{3-n}{1-n}}.} \tag{40}$$

Constant of proportionality. Solving the radius relation for ρ_c,

$$\rho_c = \left[\frac{4\pi G}{(n+1)K}\, \frac{R^2}{\xi_n^2}\right]^{\frac{n}{1-n}}, \tag{41}$$

and substituting into

$$M = 4\pi\rho_c R^3\, (-\theta'(\xi_n)/\xi_n) \tag{42}$$

yields

$$\boxed{M = \left[4\pi\,(-\theta'(\xi_n))\,\xi_n^{-\frac{1+n}{1-n}} \left(\frac{4\pi G}{n+1}\right)^{\frac{n}{1-n}}\right] K^{-\frac{n}{1-n}}\, R^{\frac{3-n}{1-n}}.} \tag{43}$$

The bracketed factor depends only on n through the Lane–Emden constants ξ_n and $\theta'(\xi_n)$, and on G.

White Dwarf Data and the Observed Mass–Radius Relation

In order to compare theoretical predictions with observations, we first analyze the white dwarf (WD) data provided in the file `white_dwarf_data.csv`. For each object, the data set contains the stellar mass in units of the solar mass and the base–10 logarithm of the surface gravity, $\log g$, in CGS units.

The stellar radius is obtained from the definition of the surface gravity,

$$g = \frac{GM}{R^2}, \tag{44}$$

which allows us to compute the radius R once the mass M and g are known. Throughout this analysis, masses are expressed in units of the solar mass $M_\odot$, while radii are expressed in units of the Earth radius $R_\oplus$, as suggested in the project description.

Using this procedure, we convert the observational data into a set of (M, R) pairs and construct the mass–radius diagram for the white dwarf sample. Figure 1 shows the resulting M–R relation in linear scale. The plot clearly demonstrates the inverse correlation between mass and radius that is characteristic of white dwarfs: more massive white dwarfs have smaller radii, reflecting the role of electron degeneracy pressure.

To better reveal possible power–law behavior, the same data are also shown in logarithmic scale. Figure 2 displays the mass–radius relation in a log–log plot. In this representation, the low–mass end of the distribution is well approximated by a straight line, indicating an underlying power–law relation between mass and radius. This behavior is expected from polytropic models and motivates the low–mass approximation discussed in the next section.

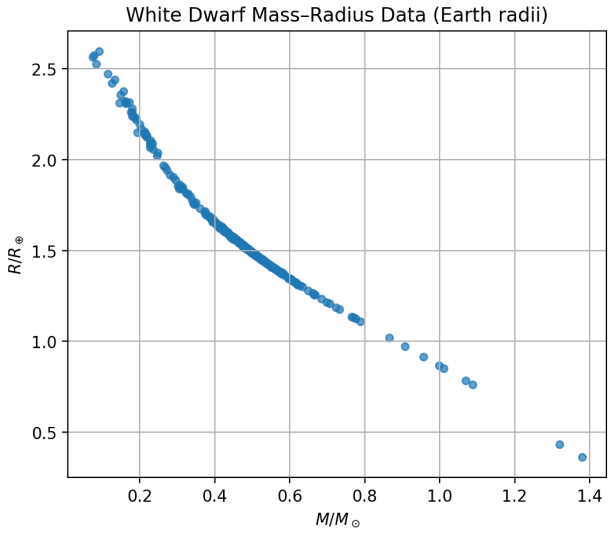

FIG. 1. Observed mass–radius relation for the white dwarf sample in linear scale. Masses are shown in units of $M_\odot$ and radii in units of $R_\oplus$.

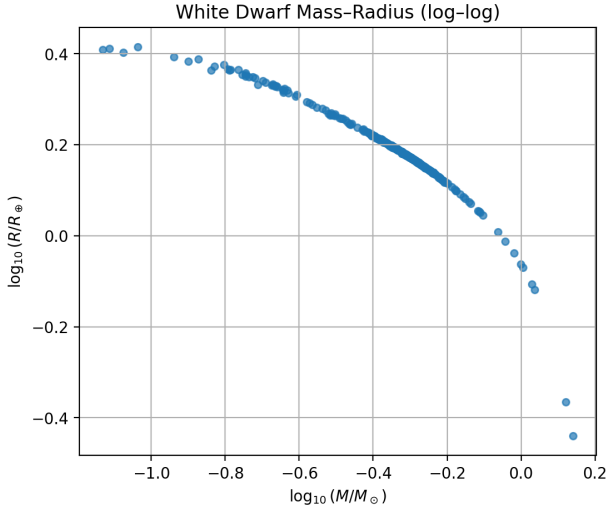

FIG. 2. Log–log plot of the observed white dwarf mass–radius relation. The approximately linear trend at low masses suggests a power–law behavior.

Low-Mass Approximation and Effective Polytropic Index

In the low-mass regime, white dwarfs are well described by a polytropic equation of state,

$$P = K^* \rho^{\gamma^*}, \qquad \gamma^* = 1 + \frac{1}{n^*}, \tag{45}$$

where n^* is an effective polytropic index and K^* is a constant.

For a polytropic star, the Lane–Emden scalings imply

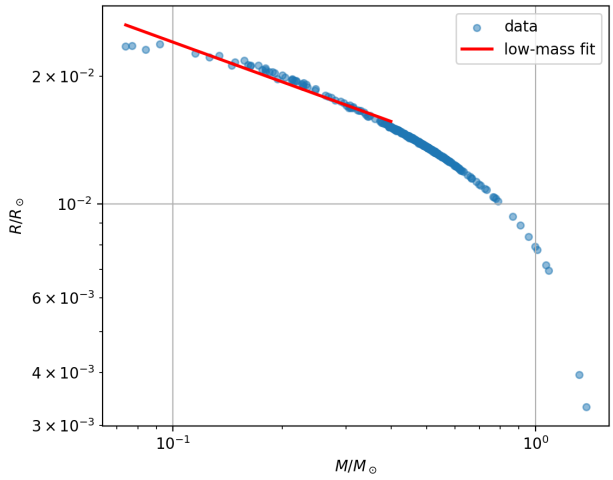

FIG. 3. Low-mass subset in log–log space with best-fit power law $R = C\,M^{\alpha}$. The fit gives $\alpha = -0.3108$, implying $n^* = 1.474$ via Eq. (49).

a power-law relation between the stellar mass and radius,

$$M \propto R^{\frac{3-n^*}{1-n^*}}. \tag{46}$$

Equivalently, this relation can be written in the form

$$R \propto M^{\alpha}, \tag{47}$$

with the slope

$$\alpha = \frac{1-n^*}{3-n^*}. \tag{48}$$

Solving for the effective polytropic index yields

$$\boxed{n^* = \frac{1-3\alpha}{1-\alpha}.} \tag{49}$$

Using the low-mass subset of the white dwarf data, a linear fit is performed in log–log space according to Eq. (47). The resulting slope α determines the effective polytropic index n^* via Eq. (49). From the fit, we obtain

$$\alpha = -0.311, \qquad n^* = 1.47, \qquad \gamma^* = 1.68. \tag{50}$$

The project further relates the effective index n^* to the parameter q appearing in the microscopic equation of state through

$$n^* = \frac{q}{5-q}. \tag{51}$$

Using the fitted value of n^*, we find $q \simeq 3$, consistent with the theoretical expectation that q is an integer.

Finally, the effective polytropic constant K^* is inferred from the normalization of the mass–radius relation. For the low-mass sample, we find

$$\log_{10} K^* \simeq 12.39, \tag{52}$$

with a relatively small scatter.

Newtonian White Dwarfs with the Full Degenerate-Electron EOS

In the low-mass regime the white dwarf EOS can be approximated by an effective polytrope, but across the full density range we must use the full cold degenerate-electron EOS,

$$P(\rho) = C\left[x(2x^2-3)\sqrt{x^2+1} + 3\sinh^{-1}(x)\right], \qquad x = \left(\frac{\rho}{D}\right)^{1/q}. \tag{53}$$

From the low-mass analysis we obtain

$$\gamma^* = 1.67835, \qquad q = 2.97911 \simeq 3, \qquad K^* = 2.48499 \times 10^{12}\ \text{(cgs)}. \tag{54}$$

Using the low-density expansion (polytropic limit), the EOS parameters satisfy

$$K^* = \frac{8C}{5D^{5/q}}. \tag{55}$$

This produces

$$C = 6.00233 \times 10^{22}\ \text{(cgs)}, \qquad \log_{10} C = 22.7783. \tag{56}$$

We also obtain two consistent estimates for D:

$$D_{\text{theory}} = 1.94786 \times 10^6\ \text{g/cm}^3, \qquad D_{\text{from } K^*} = 2.03253 \times 10^6\ \text{g/cm}^3, \tag{57}$$

with agreement at the few-percent level ($D_{\text{from } K^*}/D_{\text{theory}} = 1.0435$).

Direct numerical integration (no Lane–Emden)

Because Eq. (53) is not globally polytropic, the Lane–Emden reduction is not applicable. Instead we solve the Newtonian structure equations directly:

$$\frac{dm}{dr} = 4\pi r^2 \rho, \qquad \frac{dP}{dr} = -\frac{Gm\rho}{r^2}. \tag{58}$$

For each chosen central density ρ_c, we integrate outward from

$$m(0) = 0, \qquad \rho(0) = \rho_c, \tag{59}$$

using Eq. (53) to convert between P and ρ during the integration. The integration is stopped when $\rho(r)$ reaches zero; this defines the stellar radius R and total mass M. For example, for $\rho_c = 10^6\ \text{g/cm}^3$ we obtain

$$\frac{M}{M_\odot} = 0.3544, \qquad \frac{R}{R_\odot} = 0.01492. \tag{60}$$

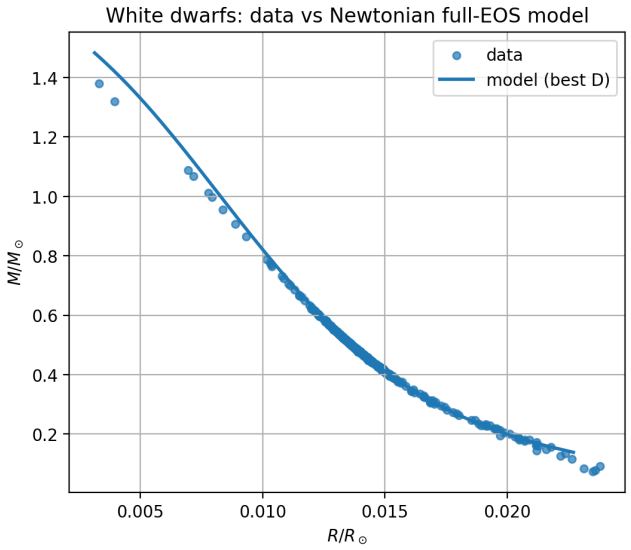

FIG. 4. Observed white dwarf mass–radius data compared with the Newtonian full-EOS model evaluated at the best-fit parameter D_{best}.

Fitting D to the observed M–R data

The observational sample contains $N = 378$ stars spanning

$$R/R_\odot \in [0.00332,\ 0.02379], \qquad M/M_\odot \in [0.074,\ 1.38]. \tag{61}$$

For a fixed trial value of D, we compute a model M–R curve by sampling a set of central densities ρ_c and generating points $(R(\rho_c), M(\rho_c))$. We then interpolate the model curve to evaluate $M_{\text{model}}(R_i)$ at each observed radius R_i and define an RMS error

$$\text{RMS}(D) = \sqrt{\frac{1}{N}\sum_{i=1}^{N}\left[M_{\text{model}}(R_i; D) - M_i\right]^2}. \tag{62}$$

We performed a coarse scan over D (ten values) followed by a refined scan around the minimum. The coarse scan already shows a pronounced minimum near $D \approx 2.0 \times 10^6\ \text{g/cm}^3$; the smallest coarse RMS occurs at

$$D = 1.96478 \times 10^6\ \text{g/cm}^3 \quad \text{with} \quad \text{RMS} = 9.39 \times 10^{-3}. \tag{63}$$

Refining around this region yields the best-fit value

$$\boxed{D_{\text{best}} = 1.95823 \times 10^6\ \text{g/cm}^3, \qquad \text{RMS}_{\text{best}} = 9.89 \times 10^{-3}.} \tag{64}$$

This best-fit value is consistent with the theoretical expectation:

$$\frac{D_{\text{best}}}{D_{\text{theory}}} = 1.0053. \tag{65}$$

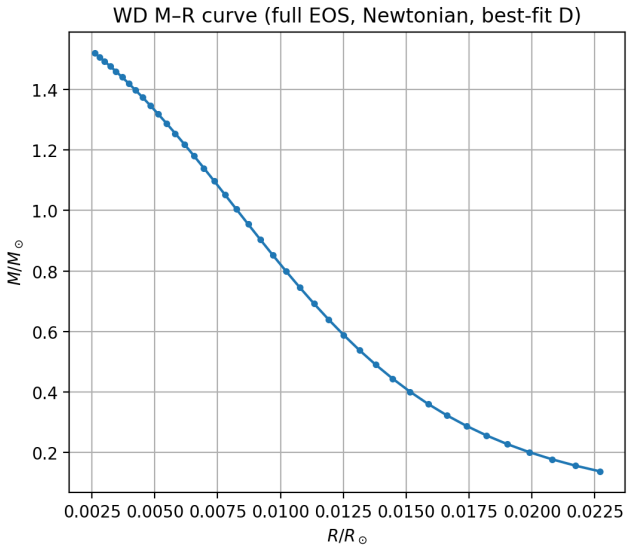

FIG. 5. Newtonian mass–radius curve generated using the full EOS at the best-fit value $D_{\rm best}$ by scanning over central density.

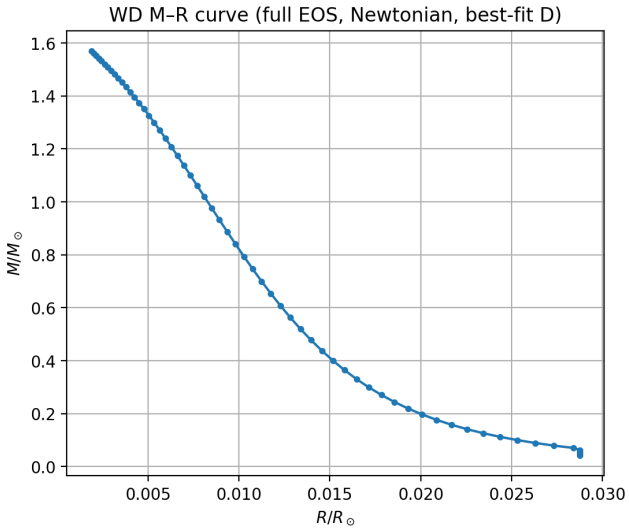

FIG. 6. Full Newtonian mass–radius relation for white dwarfs obtained using the full degenerate-electron EOS at the best-fit value $D_{\rm best}$. The curve shows the emergence of a maximum mass at high central density.

High-density limit and maximum mass in the scan

At high densities the EOS approaches the relativistic degenerate limit, for which the effective adiabatic index tends toward $\gamma \to 4/3$. Numerically, the effective index inferred at high densities approaches

$$\gamma_{\rm eff} \approx 1.34\text{–}1.37, \tag{66}$$

consistent with the expected trend toward 4/3.

Scanning over sufficiently large ρ_c produces an upper envelope in the Newtonian full-EOS mass–radius curve. The maximum mass reported from our (best-fit D) scan is

$$M_{\rm max} \approx 1.51\, M_\odot \quad \text{at} \quad \rho_c \approx 3.16 \times 10^9 \ \text{g/cm}^3, \tag{67}$$

within the explored range of ρ_c.

Existence of a Maximum Mass and the Chandrasekhar Limit

The numerical integration of the Newtonian stellar structure equations using the full degenerate-electron equation of state produces a complete mass–radius relation for white dwarfs. Figure 6 shows the resulting $M(R)$ curve obtained by scanning the central density in the range $\rho_c \in [10^4, 10^{10}]$ g/cm^3 using the best-fit value $D_{\rm best}$. The curve exhibits a clear maximum mass,

$$M_{\rm max} \simeq 1.57\, M_\odot, \tag{68}$$

beyond which increasing the central density leads to decreasing stellar radius without further increase in mass.

The existence of this maximum mass can be understood analytically by examining the ultra-relativistic limit of the equation of state. In the limit $x \gg 1$, a series expansion of the EOS yields the leading-order behavior

$$P(\rho) \simeq \frac{2C}{D^{4/3}}\, \rho^{4/3}, \tag{69}$$

which corresponds to a polytropic equation of state with index $n = 3$.

The constants appearing in the EOS are given by

$$C = \frac{m_e^4 c^5}{24\pi^2 \hbar^3}, \qquad D = \frac{\mu_e m_u m_e^3 c^3}{3\pi^2 \hbar^3}, \tag{70}$$

where m_e is the electron mass, m_u is the atomic mass unit, and μ_e is the number of nucleons per electron.

For an $n = 3$ polytrope, the total mass is independent of the central density. Using the polytropic mass formula, the Chandrasekhar mass can be written as

$$M_{\rm Ch} = 4\pi\, \omega_3 \left(\frac{4}{4\pi G} \frac{2C}{D^{4/3}} \right)^{3/2}, \tag{71}$$

where $\omega_3 = -\xi_1^2 \theta'(\xi_1)$ is the Lane–Emden constant for $n = 3$.

NEUTRON STARS IN GENERAL RELATIVITY

Relativistic stellar structure and TOV equations

In the relativistic regime, hydrostatic equilibrium must be described within general relativity. Assuming a

static, spherically symmetric spacetime and a perfect-fluid stress–energy tensor, the stellar interior is governed by the Tolman–Oppenheimer–Volkoff (TOV) equations,

$$\frac{dm}{dr} = 4\pi r^2 \rho, \tag{72}$$

$$\frac{dP}{dr} = -\frac{G}{r^2}\frac{\left(\rho + \frac{P}{c^2}\right)\left(m + 4\pi r^3 \frac{P}{c^2}\right)}{1 - \frac{2Gm}{rc^2}}. \tag{73}$$

Compared to the Newtonian hydrostatic equilibrium equation, relativistic corrections arise from three distinct effects: (i) pressure contributes to the inertial mass density, (ii) pressure contributes directly to the gravitational field, and (iii) strong-field corrections enter through the redshift factor $1 - 2Gm/(rc^2)$.

Given an equation of state $P(\rho)$, Eqs. (72) and (73) are integrated outward from a chosen central density ρ_c with initial conditions

$$m(0) = 0, \qquad \rho(0) = \rho_c. \tag{74}$$

The integration is terminated at the radius R where $P(R) = 0$, defining the stellar radius and the gravitational mass $M = m(R)$. Repeating this procedure for a range of central densities produces a family of equilibrium configurations.

Mass–radius relation and existence of a maximum mass

The mass–radius relation obtained from the numerical integration of the TOV equations is shown in Fig. 7. Unlike the Newtonian case, the relativistic $M(R)$ curve exhibits a clear maximum mass. From the numerical results, we find

$$M_{\max} \simeq 0.084\, M_\odot \quad \text{at} \quad R \simeq 12 \text{ km}, \quad \rho_c \simeq 1.0 \times 10^{18} \text{ kg/m}^3. \tag{75}$$

Beyond this point, increasing the central density no longer increases the total mass. This behavior is a direct consequence of relativistic gravity: at high compactness, the gravitational role of pressure and spacetime curvature outweighs the additional support provided by increasing density.

Stability analysis from the mass–central-density relation

The stability of relativistic stellar configurations can be assessed using the turning-point criterion. Along the stable branch of solutions, increasing the central density leads to an increase in the total mass, corresponding to $dM/d\rho_c > 0$. At the maximum mass, $dM/d\rho_c = 0$, and for larger central densities the slope becomes negative, signaling the onset of instability. This criterion

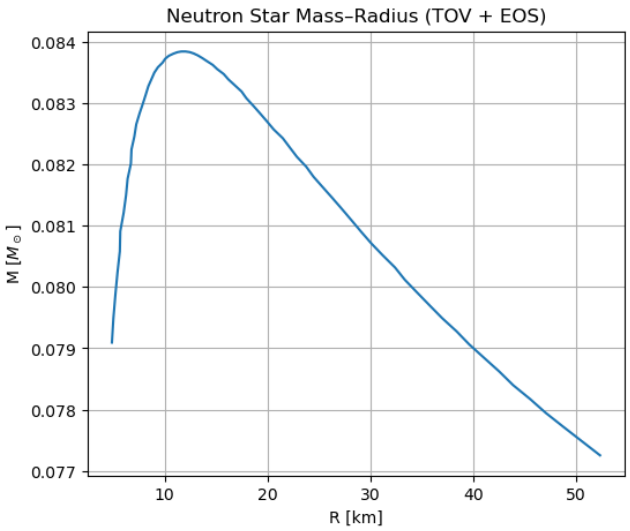

FIG. 7. Neutron star mass–radius relation obtained from the TOV equations using the adopted equation of state.

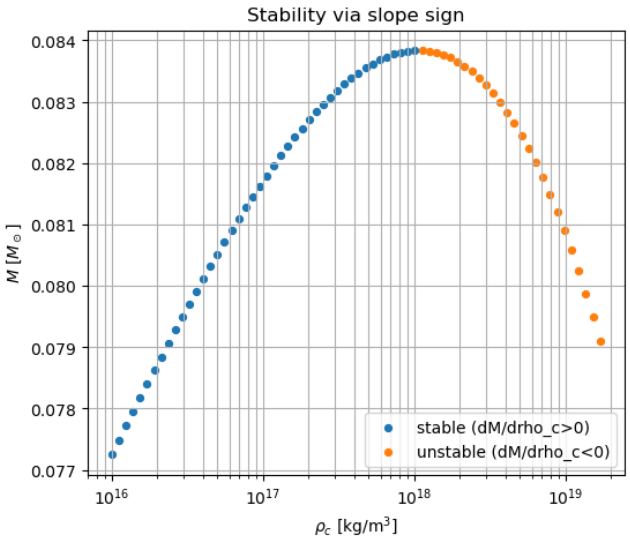

FIG. 8. Stability of TOV solutions classified according to the sign of $dM/d\rho_c$.

is confirmed by the numerical $M(\rho_c)$ relation and the associated stability classification shown in Fig. 8. The maximum mass therefore marks the boundary between stable and unstable neutron star configurations.

Gravitational binding energy and proper mass

In general relativity, the gravitational mass M differs from the proper (rest) mass M_P due to gravitational binding. The proper mass is obtained by integrating the

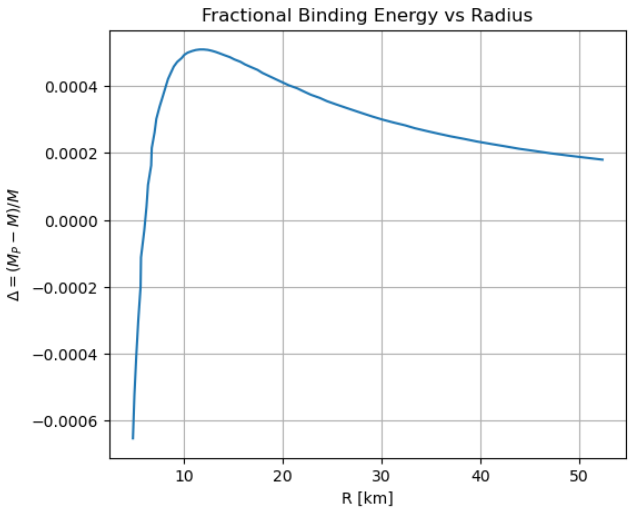

FIG. 9. Fractional binding energy as a function of stellar radius.

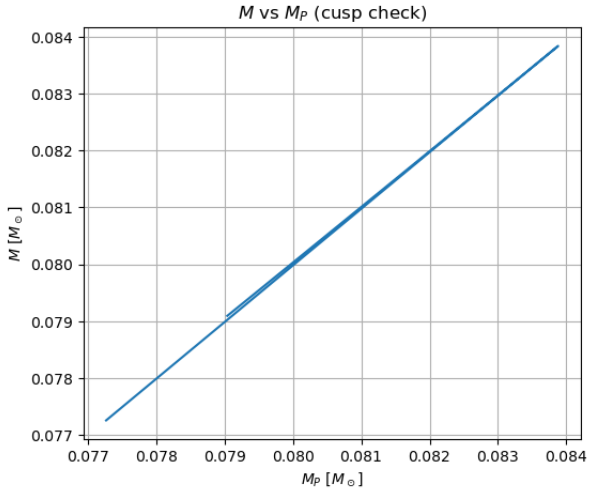

FIG. 10. Gravitational mass versus proper mass for the TOV sequence.

rest-mass density over the proper volume,

$$M_P = \int_0^R 4\pi r^2 \rho(r) \left(1 - \frac{2Gm(r)}{rc^2}\right)^{-1/2} dr. \tag{76}$$

The fractional binding energy is defined as

$$\Delta = \frac{M_P - M}{M}. \tag{77}$$

Figure 9 shows that more compact stars exhibit larger binding energy, reflecting the increasing importance of relativistic effects. The smooth relation between M and M_P shown in Fig. 10 provides an internal consistency check of the numerical integration.

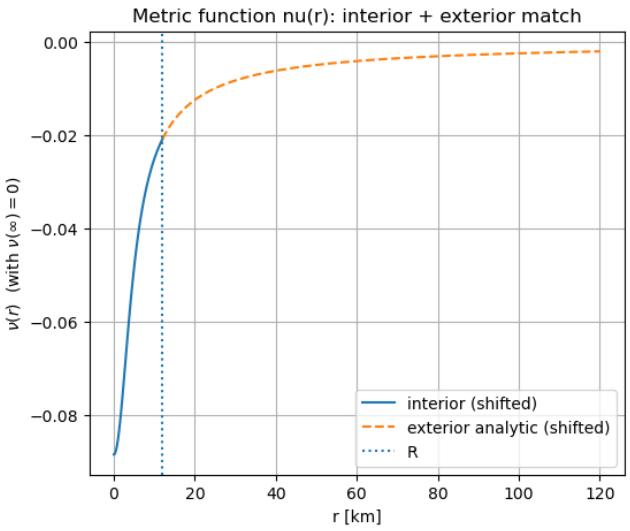

FIG. 11. Metric function $\nu(r)$ for the interior solution matched to the exterior Schwarzschild spacetime at the stellar radius.

Interior metric and exterior Schwarzschild matching

The spacetime metric inside the star is described by the function $\nu(r)$, which satisfies

$$\frac{d\nu}{dr} = \frac{2G}{c^2} \frac{m(r) + 4\pi r^3 P(r)/c^2}{r^2 \left(1 - \frac{2Gm(r)}{rc^2}\right)}. \tag{78}$$

The integration constant corresponds to a rescaling of the time coordinate and is fixed by matching the interior solution to the exterior spacetime. The numerical interior solution for $\nu(r)$ matches smoothly to the exterior Schwarzschild solution at the stellar surface. The central gravitational time dilation is quantified by $e^{\nu(0)/2} \simeq 0.96$.

Outside the star there is no matter, so that $P(r > R) = 0$ and $m(r > R) = M$. In this region, the remaining Einstein equation reduces to

$$\nu'(r) = \frac{2M}{r(r - 2M)}, \qquad r > R. \tag{79}$$

Using *Mathematica*, this equation can be integrated analytically. Imposing the continuity of $\nu(r)$ in $r = R$ yields

$$\nu(r > R) = \ln\left(1 - \frac{2M}{r}\right) - \ln\left(1 - \frac{2M}{R}\right) + \nu(R), \tag{80}$$

confirming that the numerical interior solution matches the analytic exterior Schwarzschild metric.

Dependence of the maximum mass on EOS stiffness

Finally, the sensitivity of the maximum mass to the stiffness of the equation of state was investigated by

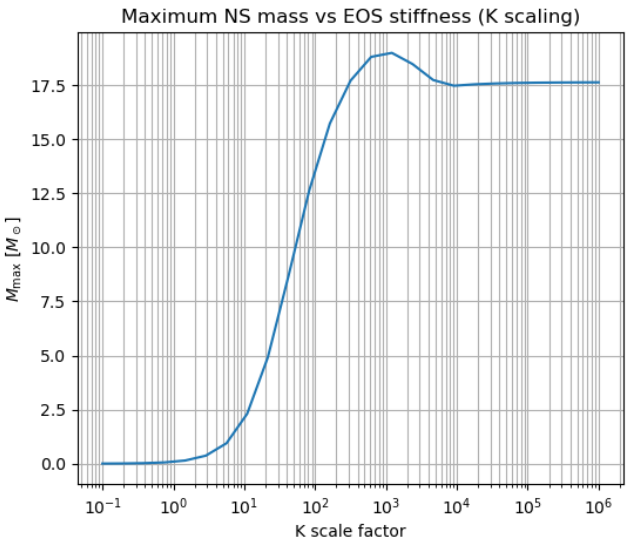

FIG. 12. Maximum neutron star mass as a function of EOS stiffness scaling parameter $K_{\rm scale}$.

rescaling the EOS normalization parameter K. Repeating the TOV integration for different values of the scaling parameter $K_{\rm scale}$ yields the relation shown in Fig. 12. The stiffer state equations support larger maximum masses; from the numerical results, a minimum scaling $K_{\rm scale} \simeq 11.6$ is required to obtain $M_{\rm max} \gtrsim 2.5\,M_\odot$..

CONCLUSION

In this project, we studied the structure of compact stars using both Newtonian gravity and general relativity. In the Newtonian framework, we derived the Lane–Emden equation for polytropic equations of state and analyzed its solutions. We examined the regularity of the solution at the center, obtained the mass–radius scaling relations, and compared these theoretical predictions with observational white dwarf data. Using the full equation of state, we performed direct numerical integrations of the Newtonian structure equations and constructed a complete mass–radius relation, which exhibits a maximum mass.

In the relativistic part, we modeled neutron stars using the Tolman–Oppenheimer–Volkoff equations. The resulting mass–radius relation shows a clear maximum mass and a transition from stable to unstable configurations, illustrating the impact of relativistic gravity. We also verified that the interior metric matches smoothly with the exterior Schwarzschild solution.